Journal of Building Engineering 98 (2024) 111259

Contents lists available at ScienceDirect

Journal of Building Engineering

journal homepage: www.elsevier.com/locate/jobe

Enhanced thermal performance of phase change mortar using multi-scale carbon-based materials

Xiaonan Wang [a,b], Yuhan Huang [a], Long Shi [c], Shishun Zhang [d], Wengui Li [b,*]

[a] School of Civil and Environmental Engineering, University of Technology Sydney, NSW, 2007, Australia
[b] Centre for Infrastructure Engineering and Safety, School of Civil and Environmental Engineering, The University of New South Wales, NSW, 2052, Australia
[c] State Key Laboratory of Fire Science, University of Science and Technology of China, Anhui, 230026, China
[d] School of Civil and Hydraulic Engineering, Huazhong University of Science and Technology, Wuhan, 430074, China

ARTICLE INFO

Keywords:
Phase change material
Energy-saving
Carbon-based materials
Temperature regulation
Thermal conductivity

ABSTRACT

Incorporating phase change material (PCM) into construction materials is an effective method for modifying building energy regulations throughout their service life. However, the effectiveness of PCM is constrained by its low thermal conductivity, highlighting the need for efficient enhancement methods. This study introduces thermally conductive carbon-based additions at both the nano-scale and meso-scale with different shapes, including carbon nano-tube (CNT), carbon black nano-particle (CB), and carbon fibre (CF) in PCM mortar. The mixed hydrated inorganic salt serves as the core PCM, while expanded perlite acts as the supporting material for the stable PCM composite, based on the presented research. The multi-scale additions establish thermal conduction pathways that improve temperature regulation performance. The modified samples exhibited a temperature difference of 2.2 °C and a time lag of up to 20 min under natural cooling conditions. Notably, CB positively influenced thermal conductivity, while CNT demonstrated an unexpected minor reduction. The enhancement in thermal conductivity increased with the content of CB, reaching an optimal enhancement of 18 %, except at a CNT content of 0.5 %. Conversely, both CB and CNT consistently improved thermal diffusivity. Furthermore, the compressive strength of the modified samples was significantly enhanced by up to 24 % compared to PCM mortar without carbon modifications. The modification method proposed in this study significantly improves both the thermal and mechanical properties of PCM mortar.

Abbreviation

T_C	Thermal conductivity
T_D	Thermal diffusivity
CB	Carbon black nano-particle
CF	Carbon fibre
CNT	Carbon nano-tube
EP	Expanded perlite
GNP	Graphene nanoplatelet

(*continued on next page*)

* Corresponding author. Centre for Infrastructure Engineering and Safety, School of Civil and Environmental Engineering, The University of New South Wales, NSW, 2052, Australia.
E-mail address: wengui.li@unsw.edu.au (W. Li).

https://doi.org/10.1016/j.jobe.2024.111259
Received 11 July 2024; Received in revised form 8 October 2024; Accepted 5 November 2024
Available online 6 November 2024

(*continued*)

NHP	$Na_2HPO_4{\cdot}12H_2O$
NS	$Na_2SO_4{\cdot}10H_2O$
PCM	Phase change material

1. Introduction

Improving energy effectiveness and reducing energy consumption are currently major global challenges, exacerbated by rapid urbanisation in the construction sector. Scholars have introduced innovative technologies, such as sustainable material [1], novel energy management methods [2] and effective construction technology [3], to address these issues. Phase change materials (PCMs) can regulate thermal energy by absorbing and releasing heat, contributing to energy-saving [4] and CO_2 reduction [5], which leads to cost-savings [6] and environmental protection [7]. Compared to altered thermal parameters, the phase change phenomenon demonstrates remarkable capacity for heat transfer regulation [8]. As a primary component of buildings, cement-based materials and structures serve as significant applications for PCMs and have exhibited strong performance [9]. The benefits of PCMs have been validated worldwide using various [10]. For instance, Zhang et al. [11] filled the cavities of concrete masonry unit blocks with insulation materials and PCMs. When the melting range matched ambient temperature, the effectiveness of PCMs in enhancing temperature inertia and energy storage was substantial. Khdair et al. [8] calculated a case in Riyadh that incorporated PCMs in the walls and ceilings, with a melting temperature of 22–24 °C. Although only a slight enhancement was observed from July to September, the annual energy saving reached 35 % with a PCM layer thickness of 20 cm. García-Pérez et al. [12] applied a PCM layer with a phase change point of 22–26 °C in a hollow block wall in Merida, Mexico. The 10-mm thick PCM layer reduced heat flux by 48.7 % during the hottest days. The optimal monthly CO_2 reduction reached 56.4 % in January and provided an annual value of 25.1 %. These research findings showcase various effective application methods for PCMs. However, the overall performance remains below optimal levels. Baylis and Cruickshank [13] analysed the economic performance and lifecycle carbon emissions of PCMs in three North American cities (Houston, Ottawa and Yellowknife). The challenging climates in these regions enabled PCMs to operate more effectively, resulting in greater reductions in carbon emissions. Importantly, the economic payback period may exceed the house's lifespan if the efficiency is low, indicating a need for further development in PCM applications.

Several factors influence the performance of PCM composites, with thermal conductivity being a critical one. Typically, both PCM and cement-based materials exhibit low thermal conductivity, which limits the optimal performance of PCMs [14,15]. Various methods exist to enhance the thermal properties of PCM applications, including modified surface configurations [16], fins [17], amorphous insertions [18], and particles [19]. Adding particles with high thermal conductivities is a prominent approach in cementitious materials. Currently, carbon-based materials are well-regarded for their thermal conductivity and are extensively used in PCM applications [20]. Li et al. [21] developed an aerogel using carbon nanotubes (CNT) and graphene oxide (GO), achieving a PCM loading ratio of 97.6 % with excellent stability and almost double the thermal conductivity. Furthermore, carbon-based additives, like CNT and carbon fibre (CF), enhance the strength of concrete [22,23] while maintaining good compatibility. This synergy enables the comprehensive advantages of carbon-modified functional materials in PCM concrete. However, understanding and modifying the thermal conductivity of concrete presents significant challenges [24], particularly due to complex structures such as interfaces, defects, and multi-phase composites.

The research on carbon additions in PCM applications has yielded significant achievements. Fikri et al. [25] demonstrated that 1 wt % CNT resulted in a thermal conductivity enhancement of 109.5 %. This enhancement increased to 150.7 % when CNTs were coupled with -COOH groups. While the melting point and latent heat showed minimal changes, the composite remained stable up to 200 °C. Haider et al. [26] used CNTs to improve thermal efficiency, with results indicating enhanced fatigue resistance and strength, attributed to a denser structure. Xu and Li [27] confirmed that CNTs improved heat storage and release rates, with no adverse effects on thermal properties, chemical compatibility, or thermal stability. Fan et al. [28] employed nano-carbon black (CB) and fins to enhance the efficiency of photothermal conversion and storage of PCM. While the scattering effect at the interface hindered heat transfer, the conductive channel was established by CB. Mishra et al. [29] found a significant increase in the thermal conductivity of lauric acid caused by CB addition. They explained it by the small primary nodule size, superior volume-filling capacity, and excellent compressibility of CB, which created tightly bound interconnected networks. Guo et al. [30] added CF with a length of 6 mm into PCM/sulphoaluminate cement paste. At a loading of 1 wt% CF, notable improvements in thermal conductivity and mechanical properties were observed, with increases of 15.1 % and 65 % at 30 °C, respectively. Singh et al. [31] also demonstrated an enhancement in the thermal conductivity of nano-scale CF, which reached 29.2 % at 2 wt%. This CF effectively compensated for strength loss because of functional modification [32]. Different additives exhibit specific intrinsic properties. One unique characteristic of CB is its filling ability, which enables it to cooperate with various materials to form a functional pathway [33]. Millimeter-scale CF has a better ability to bridge cracks and provide a longer thermally conductive path.

Compared to single two-dimensional materials, three-dimensional structures provide significant enhancements. Zhou et al. [34] prepared a graphite nanosheets-based carbon foam to support stearic acid. While carbon-based supporting materials are primarily utilised in areas such as batteries, their application in fabricating PCM composites is gaining interest [35]. Utilising them as supporting materials can enhance compatibility [20,27,36,37]. However, these materials often serve merely as additives in raw PCM and concrete, rather than delete as supporting structures for PCM composites. In addition to the direct application of three-dimensional materials, integrating multi-dimensional materials can also improve spatial performance and foster novel enhancements [21].

Atinafu et al. [38] created a hybrid scaffold by synthesising CNT and exfoliated graphene nanoplatelet (GNP) to support PCM. Compared with CNT/PCM, the proposed PCM composite exhibited a higher loading ratio (increasing from 51.1 % to 79.9 %), greater latent heat (from 96.6 J/g to 150.9 J/g), and a reduction in supercooling (from 44.2 % to 56.6 %). Ramakrishnan et al. [39] separately coated 5 wt% of CNT and GNP in PCM. The thermal conductivities of the mortar increased by 30 % and 49 %, resulting in higher stored energy, which rose by 122 % and 200 %, respectively. Therefore, this paper hopes to improve the comprehensive performance of PCM concrete through the cooperation of carbon additions with various shapes and scales, which may achieve a similar effect to 3D material [53–55].

One of the current key developments in this field is the enhancement of thermal conduction and the maintenance of mechanical strength, with carbon-based additions showing significant potential. The CB and CNT are representative examples of zero-dimensional and one-dimensional nanomaterials, respectively [33]. Millimetric-scale CF is also widely used to improve strength [32]. This study designs hybrid carbon-based material additions to enhance both thermal and mechanical properties, providing a method for reliable PCM mortar applications. CB and CNT, with their varying dimensions, establish spatial connections that improve thermal transfer and energy storage performance. In addition to the strength benefits provided by CNT, CF contributes to modifications at a macroscopic scale, creating channels within the nanoscale thermal conductive network [56–60].

This paper begins with the preparation details in Section 2, which introduces the selection and properties of raw materials, followed by the procedure for fabricating PCM composites and mortar. Section 3 outlines the testing methodology used to assess significant performance metrics. The “free thermal convection” test directly reflects performance in the laboratory, while the other tests aim to elucidate underlying mechanisms. Section 4 presents and analyses the testing results, covering macro-performance in terms of thermal properties as well as chemical and physical characteristics. Valuable findings and analyses are summarized in Section 5, while Section 6 offers several suggestions for further research, assisting readers and researchers in exploring new ideas on this topic.

2. Material and preparation

2.1. Raw materials selection and properties

The aggregate used in this study was EP with particle sizes primarily ranging from 0.3 to 1.3 mm, sourced from the Australian company Ausperl. This aggregate features a porous structure and has a dry density of 70 kg/m^3. Prior to the experiment, the aggregate was dried to eliminate any moisture. The silica sand (SS) used in the mixture had a similar particle size to that of the EP but differed in structure. Portland cement was obtained from Cement Australia Pty. Ltd., with up to 50 % of the particles measuring less than 10 μm. Additionally, a polycarboxylate-based superplasticiser (Visco Crete) was employed to enhance flowability.

Hydrated inorganic salts were used as PCMs in this experiment. Sodium hydrogen phosphate dodecahydrate ($Na_2HPO_4{\cdot}12H_2O$, NHP) [40] and sodium sulphate decahydrate ($Na_2SO_4{\cdot}10H_2O$, NS) [14] were selected. All raw materials were analytical reagents with a purity of 99 %. The NHP and NS were pre-melted in equal masses to create the binary PCM. The mixing procedure was conducted in sealed tubes within a warm tank maintained at 60 °C, using ultrasonic vibration.

For this experiment, multi-wall CNT was chosen, with an external diameter ranging from 8 to 15 nm and a length of 8–14 μm [41]. The CB had an average particle size of 40 nm and a compacted density of ~300 g/L [42]. CF had a significantly larger size, with a diameter of 7 μm and a length of 5 mm, exhibiting a good tensile strength of 4.5 GPa. The specified parameters were provided by the manufacturers.

2.2. Sample preparation

In addition to direct addition methods [43,44], the most widely adopted approaches for incorporating PCMs are micro-encapsulation, macro-encapsulation, and shape stabilisation, resulting in microPCM, macroPCM, and SSPCM, respectively [45]. These methods enhance compatibility under challenging conditions. All three techniques have demonstrated significant effectiveness in maintaining the energy storage capabilities of PCMs across various applications. Shape stabilisation is an economical and stable method for PCM loading, particularly applied in concrete and mortar [46]. Expanded perlite (EP) is a versatile raw material commonly

Table 1
Raw material proportion for mortar samples.

Specimen	Cement (g)	Water/c	SS/c	EP/c	EPC/c	SP/c	CNT/c	CF/c	CB/c
SE0	2000	0.46	1:1	6 %	–	0.5 %	0 %	0 %	0 %
SC0	2000	0.46	1:1	–	16 %	0.5 %	0 %	0 %	0 %
SC1-25	2000	0.46	1:1	–	16 %	3.0 %	0.1 %	0.5 %	0.25 %
SC3-25	2000	0.46	1:1	–	16 %	3.5 %	0.3 %	0.5 %	0.25 %
SC5-25	2000	0.46	1:1	–	16 %	4.0 %	0.5 %	0.5 %	0.25 %
SC1-5	2000	0.46	1:1	–	16 %	3.0 %	0.1 %	0.5 %	0.50 %
SC3-5	2000	0.46	1:1	–	16 %	3.5 %	0.3 %	0.5 %	0.50 %
SC5-5	2000	0.46	1:1	–	16 %	4.5 %	0.5 %	0.5 %	0.50 %
SC1-75	2000	0.46	1:1	–	16 %	3.0 %	0.1 %	0.5 %	0.75 %
SC3-75	2000	0.46	1:1	–	16 %	4.0 %	0.3 %	0.5 %	0.75 %
SC5-75	2000	0.46	1:1	–	16 %	4.5 %	0.5 %	0.5 %	0.75 %

used in concrete and mortar to modify thermal properties, and it is also effective for PCM loading [47].

EP and binary PCM were utilised to fabricate the PCM composite. The mass ratio of PCM to EP was established at 10:6, which is equivalent to a volume ratio of 7:60. This ratio is lower than the volume porosity of EP, which is 65 %, thereby enabling stable PCM retention. The raw materials were combined in a beaker, which was then sealed with film and placed in a vacuum oven. A vacuum of 80 kPa was applied, and the temperature was maintained at 50 °C. After 6 h, the composite was allowed to cool to room temperature before being removed from the vacuum oven. Finally, the film was removed, and the solid EP/PCM composite (EPC) was extracted for use in this experiment.

The proportions of raw materials for the mortar samples used in this experiment are presented in Table 1. EP and EPC partially replaced the SS as aggregates with a volume percentage of 50 %. The reference samples, SE0 and SC0, were employed with and without PCM, respectively, and both did not contain carbon additives. All percentages in Table 1 were calculated based on mass, with “c" representing cement. For instance, SS/c denotes the mass ratio of SS to cement. Most percentages remained constant, except for CNT, CB—both critical variables for this research—and SP, which was added to compensate for the reduced flowability resulting from the increased carbon content. Flowability was controlled within the range of 20–22 cm.

The conventional mortar casting procedure was modified to accommodate the carbon additives. First, CF was thoroughly mixed with the dry materials, including cement and aggregates, in a mortar mixer at low speed. Subsequently, a portion of the water was utilised to disperse the CNT and CB. The measured CNT and CB were combined with tap water and SP, which was subjected to ultrasonic treatment for approximately 30 min to achieve complete dispersion; SP enhanced the dispersion quality. The resulting suspension was then gradually poured into the dry mixed materials, followed by slow mixing for 1 min. Next, the remaining water and SP were added, and the mixture was blended at medium speed for 2 min. Finally, the fresh mortar was cast into moulds as 50 × 50 × 50 mm cubes, adhering to the specified curing requirements [48]. Testing commenced after a curing period of 28 days.

3. Experimental methodology

3.1. Structure and ideas for the methodology

This research begins with investigating “free thermal convection,” focusing on temperature regulation under ambient conditions. Changes in the specimen temperature directly reflect thermal mass transfer, which is critical for effective thermal mass management in buildings. The key factors influencing this performance are the thermal properties of the materials; therefore, specialised equipment was employed to test two representative parameters: thermal conductivity and thermal diffusivity. Subsequently, PCM mortar was designed for construction applications, with particular attention given to mechanical performance. A series of characterisation tests were conducted to assess the properties of the PCM mortar. Differential Scanning Calorimetry (DSC) was utilised to directly evaluate thermal convection and storage during temperature fluctuations, which is significant for PCM applications. X-ray Diffraction (XRD) and Thermogravimetric Analysis (TGA) are standard methods employed to investigate the composition and thermal stability of cementitious materials, thereby providing evidence of the feasibility of PCM mortar in practical scenarios. Additionally, microstructural analysis was performed to support and elucidate the previous findings. This comprehensive approach enables us to draw reliable and well-founded conclusions regarding the performance of PCM mortar.

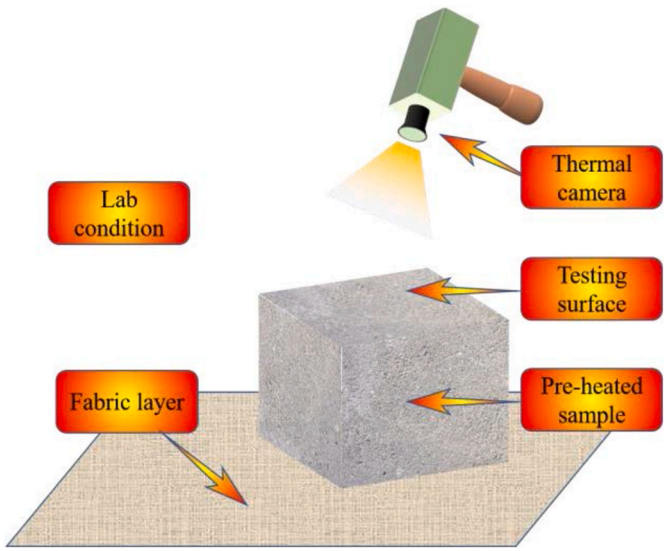

Fig. 1. Configuration for free thermal convection test.

3.2. Free thermal convection

All samples were heated in an oven at 57 °C for 4 h. This temperature ensured that PCM was in a liquid state and that latent heat was effectively stored. The testing commenced immediately after the samples were removed from the oven and continued until the temperature approached room temperature (around 25 °C). This procedure was conducted in a controlled laboratory environment. Temperature measurements were recorded using a HIKMICRO H21 infrared thermal imaging camera, which has a resolution of 256 × 192 pixels and a temperature measurement range from −20 to 350 °C. The distance between the sample and the camera was set at 0.5 m, and the testing mode was adjusted to account for the rough surface characteristic of concrete. To mitigate thermal reflection from the desk surface, a piece of fabric was placed beneath the sample. The experimental configuration is shown in Fig. 1.

3.3. Thermal properties of the cubic specimen

The thermal convection performance is affected by the intrinsic properties of the materials. The critical thermal conductivity was measured using a widely recognised Hot Disk apparatus, which employs the transient plane source method. A Kapton 5501 F2 sensor, with a radius of 6.4 mm and an output power of 10 mW, was used for this measurement. The sensor was embedded between two specimens with the same properties, as shown in Fig. 2. Testing was conducted in a laboratory environment maintained at a temperature between 22.5 and 23.5 °C. The results for thermal conductivity and thermal diffusivity were analysed.

3.4. Mechanical performance

The reduced strength of PCM concrete is a significant concern associated with the addition of PCM, and the underlying reasons are complex [49–51]. Testing the mechanical properties is essential for evaluating PCM concrete. In this experiment, a compression machine was utilised to assess the compressive strength of all cubic specimens in accordance with ASTM C109/C109M − 21, with a loading speed of 1.2 kN/s [48]. The compressive strength results for each sample were determined as the average value of five specimens. Throughout the compression testing, the room temperature was maintained at 23 °C.

3.5. Thermal, compound, and structure characteristics

Thermal properties, especially phase change performance, are critical for evaluating PCM concrete. Differential scanning calorimetry (DSC) was employed as the primary thermoanalytical technique in this experiment. The advanced NETZSCH DSC 300 Supreme, equipped with nitrogen protection gas, was used for the DSC tests. The temperature range was set between 15 and 65 °C, with a heating/cooling rate of 5 °C/min. Each test consisted of 20 heating-cooling cycles, totaling 400 min. Mortar samples weighing 20–30 mg were placed in closed aluminium crucibles.

X-Ray Diffraction (XRD) was employed to analyse the crystalline components of the cement-based materials. The crushed mortar was ground in fine powder with a size of ~20 μm at the laboratory to ensure reliable results. The powder was kept at 40 °C for 24 h to eliminate the moisture that may interfere with the laser reflection. The Bruker D8 Discover was used for the XRD tests, with a 2θ scan range of 5°–70°, encompassing a valid range for analysis. Thermal gravimetric analysis (TGA) was completed to investigate the material composition via mass change at elevated temperatures. The NETZSCH STA449 F5 Jupiter was utilised, featuring a balance resolution of 0.1 μg and a maximum chamber temperature of 1600 °C. The heating rate was set to 10 °C/min, with N_2 flowing 20 ml/min. Data collection commenced at 25 °C and concluded at 1000 °C. For each sample, 20–30 mg of powder was placed in an alumina crucible for testing.

ZEISS SUPRA-55 VP field emission scanning microscope (FE-SEM) was selected to investigate the microstructure of cement hydration products and the distribution of additives. A conductive gold layer, 10 nm thick, was coated on the observed surfaces. To

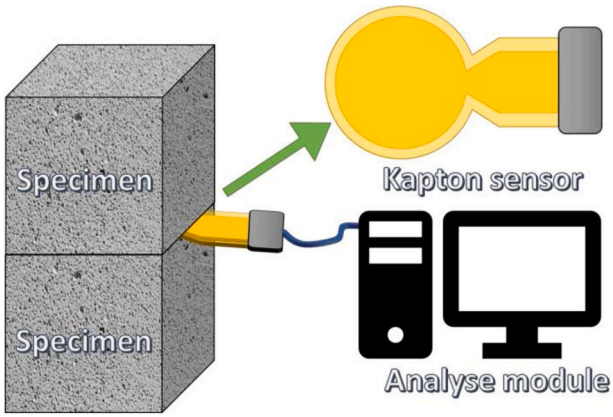

Fig. 2. Configuration for thermal conductivity test.

preserve the original features, samples were cleaned using compressed air and dried without polishing or fine cutting, despite the fact that a polished plane could enhance image quality by reducing electric charging. All samples for the SEM test were collected pieces from mechanical tests, which had been cured for 28 days and subjected to compression.

4. Results and discussions

4.1. Free thermal convection

The initial temperature was around 55 °C, which was slightly lower than the oven temperature of 57 °C due to rapid thermal convection prior to testing. The infrared camera could only capture the surface temperature, representing the cooling front. As the stored heat within the inner core gradually dissipated through the surface, this resulted in varying temperature distributions. All thermal maps had the same temperature legend that was placed on the bottom left. The maximum temperature was indicated by "X," while "N" referred to the minimum temperature. The central temperature was denoted by the green "+" symbol.

As shown in Fig. 3, all samples reached elevated temperatures within the oven. The minimum temperature was recorded in the ambient room, while the maximum temperature was measured from the sample surface. Under ideal conditions, the temperature distribution should be uniform following oven heating. However, in practice, the temperature at the edges of the samples was lower than that at the centre of the surface. This discrepancy occurred because the thermal mass was transferred from the samples to the surrounding air, resulting in a temperature reduction, while the heat within the inner core migrated toward the surface due to the established temperature gradient. The edges of the samples were influenced by multiple surfaces, leading to increased heat loss and a longer distance to the inner core, which diminished heat recovery efficiency. This phenomenon is further illustrated in Fig. 4. Additionally, during the test, there was a time delay between the removal of the samples from the oven and the temperature capture, which contributed to the aforementioned effects.

The temperatures of all samples exhibited a significant decline in the absence of oven heating, as shown in Fig. 5, which showed a maximum temperature difference of around 10 °C compared to the initial state. The substantial temperature differential between the samples and the surrounding environment, exceeding 30 °C, facilitated rapid heat transfer and heat loss, resulting in a swift decrease in temperature. The temperature distribution remained similar to that observed at the initial state; however, the area of relatively low temperature near the edges increased. After 10 min, the inner temperature gradient became more pronounced than it had been initially, aligning more closely with the patterns depicted in Fig. 4.

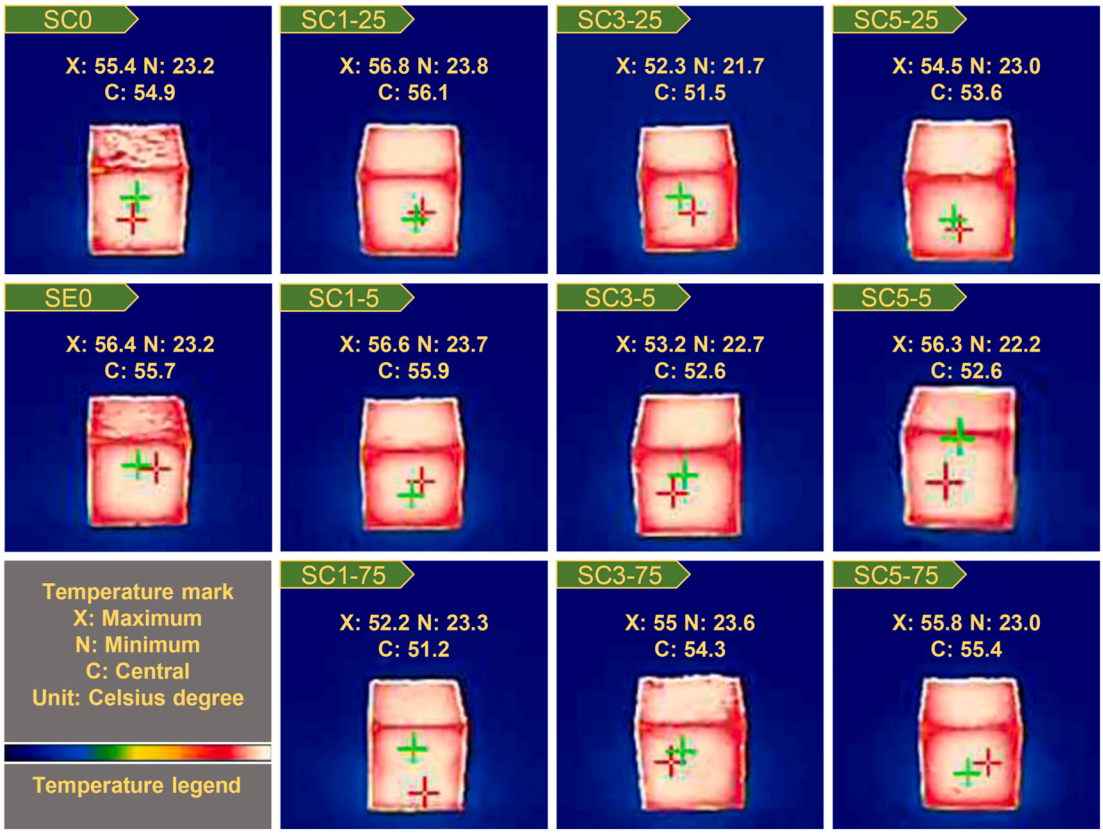

Fig. 3. Initial temperature distribution of tested specimen.

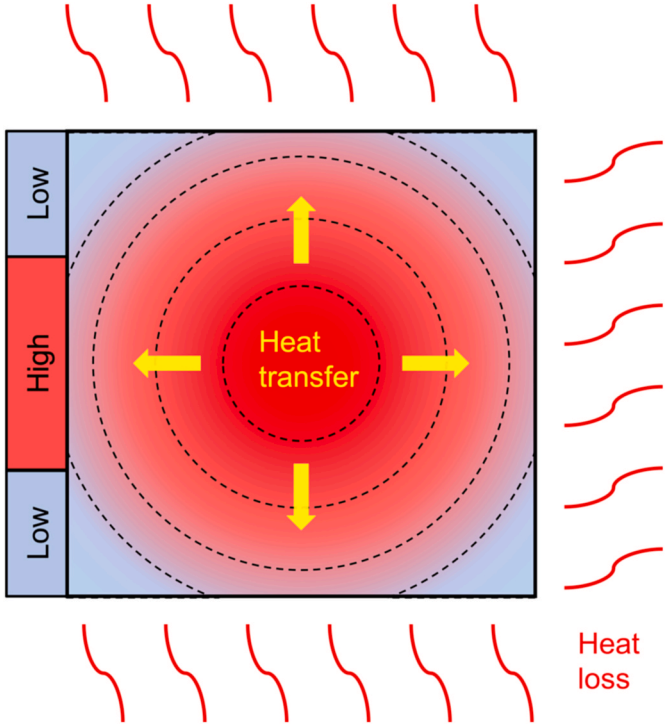

Fig. 4. Heat transfer and heat loss illustration.

As time progressed, the distinct features of the temperature distribution shown in Fig. 5 diminished, as the heat mass in the core region became insufficient. As shown in Fig. 6, most samples exhibited a uniform surface temperature, which continued to decline. At this stage, the temperature differences among the samples became more pronounced, despite being minimal at the outset. For example, the temperature difference between SE0 and SC1-5 was only 0.2 °C for both the maximum and central temperatures initially, but this difference increased to 4.2 °C, as shown in Fig. 6. According to the mixing proportion as shown in Table 1, this variation can be attributed to the presence of PCM and the various carbon additives. The former affected the original heat mass, and the latter influenced heat conduction. These details will be analysed in the following sections.

After 60 min cooling, the temperatures of the samples approached room temperature, as shown in Fig. 7. The minimum temperature shown in Figs. 3, 5 and 6 and 7 was about 23 °C but this does not reflect the room air temperature. The minimum temperature recorded in the figures was measured from the table surface, while the laboratory thermometer indicated a room temperature of around 25 °C. Therefore, it can be concluded that the surfaces of most samples reached temperatures close to room temperature.

The central temperature development with a time gap of 10 min was illustrated in Fig. 8(a). The temperatures of all samples continued to decrease and approached a stable state near room temperature. Overall, the rate of temperature decline diminished over time as the temperature difference decreased, which is the primary driving force for thermal convection. To clarify the data, several critical and representative lines were extracted. The effect of PCM is clearly illustrated in Fig. 8(b). SE0 and SC0 exhibited similar initial temperatures and rates of decrease over the first 20 min. Subsequently, a significant gap emerged, with SC0 displaying a temperature of 30.5 °C, compared to SE0's temperature of 28.8 °C. These temperatures correspond to the melting point of the PCM and the heat released during this phase change mitigated the temperature decline. The temperature gap between samples remained around 2.2 °C but decreased to 1.6 °C at 60 min, attributed to the insufficient heat retention in the PCM. In addition, the temperature lag of 10–20 min was obtained (same temperature: a. SE0 at 30 min and SC0 at 40 min; b. SE0 at 40 min and SC0 at 60 min).

Overall, the temperature decreased more rapidly due to the effect of carbon additions on thermal conductivity. However, the influence of various additives was not uniform and was not always beneficial. On the one hand, the accelerating of CB was relatively consistent across most samples, enhancing thermal convection when combined with the same concentrations of CNT and CF. On the other hand, CNT exhibited varying effects, despite being generally regarded as a thermal conductivity enhancer. For example, in the CB 5 group, as shown in Fig. 8(c), the rate of temperature decrease diminished with increasing amounts of CNT. This phenomenon was influenced by the amount of CB, and the comprehensive results are presented in Fig. 8(a).

4.2. *Thermal properties*

To analyse the performance of free thermal convection and evaluate the designed PCM mortar, crucial parameters were tested including thermal conductivity (T_C) and thermal diffusivity (T_D). As shown in Fig. 9, T_C presented moderate moderate fluctuation. SE0, representing conventional mortar, displayed a T_C of 1.368 W/(mK) while the addition of PCM resulted in a lower T_C of 1.263 W/(mK).

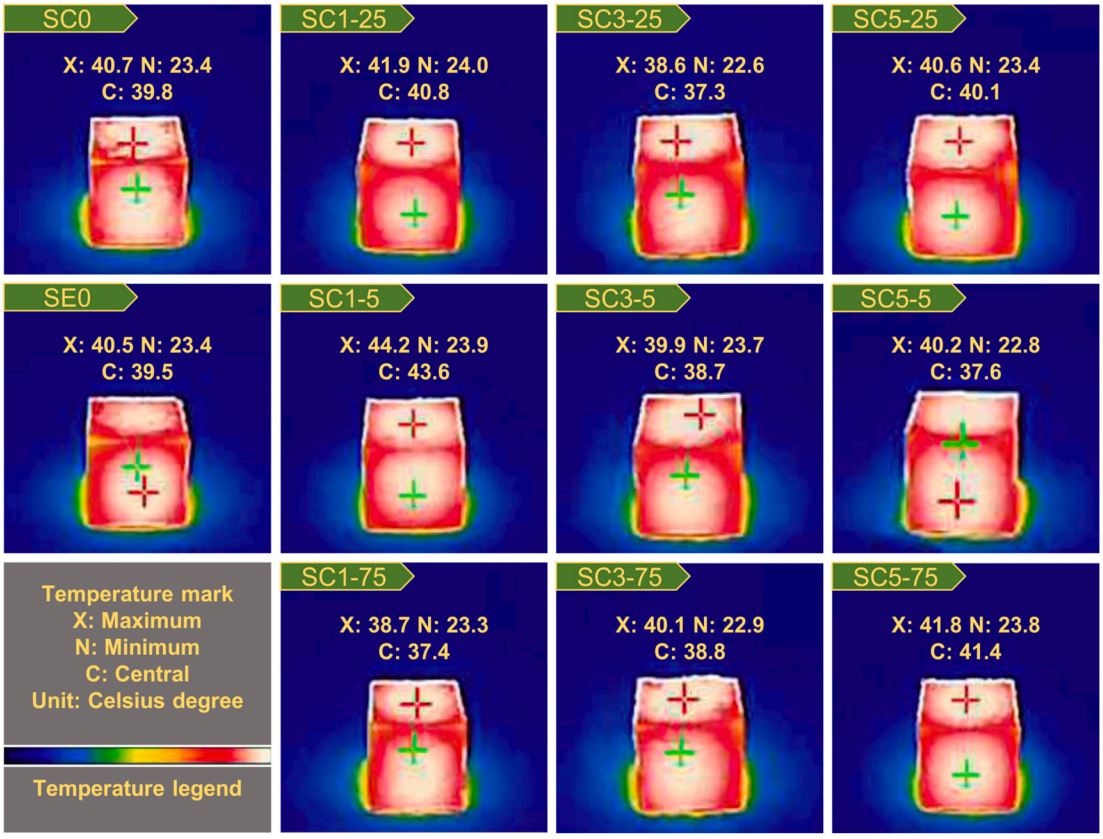

Fig. 5. Temperature distribution at 10 min cooling.

The thermal conductivity of the crystal salt used as PCM was very low and the PCM addition could weaken the contact between aggregate and cement paste. The density results are presented in Fig. 10 where SC0 demonstrated a significant reduction. SC1-75 exhibited the highest T_C of 1.488 W/(mK), with an enhancement of 18 %. While the inclusion of carbon-based materials was expected to improve T_C, the results for SC1-25 were unsatisfactory. This can be attributed to a looser structure and lower density resulting from the addition of carbon fibers (CF), which provided only marginal enhancement due to the small quantity of nano-materials Overall, the density increased with the addition of nano-materials, particularly from SC1-25 to SC1-75. Furthermore, CB generally improved the T_C except for samples containing CNT of 0.5 %, where it decreased from 1.422 W/(mK) to 1.309 W/(mK). This decrease can be explained by poor distribution of the nano-carbon materials as their quantity increased.

While CB has been shown to be beneficial for T_C, CNT sometimes exerts an adverse influence. Although pure CNT had both excellent electrical and thermal conduction, studies have indicated that their addition to concrete enhances electrical conductivity while only marginally reducing thermal conductivity [52]. The CNT strands act as energy barriers, facilitating electron transport while hindering phonon movement. This results in the scattering of lattice vibrational energy of the phonons, as shown in Fig. 11. Therefore, the influence on density and thermal conductivity were opposing (e.g., among SC1-75, SC3-75, and SC 5–75). The increase in T_C observed in SC1-25, SC3-25, and SC5-25 can primarily be attributed to a significant improvement in density. In contrast, the differences in thermal conductivity among the other samples (those containing 0.5 % and 0.75 % CB) were not compelling.

Another important parameter analysed in this study was thermal diffusivity (T_D), as shown in Fig. 12. Notably, T_D did not exhibit a strong correlation with T_C. Despite the varying impacts on T_C, the improvement in T_D with the incorporation of additional carbon materials was noteworthy. The uptrend in T_D persisted up to SC5-25, with values increasing from 0.6 to 1.42 mm^2/s, resulting in a notable difference of 136 %. While CNT did not directly demonstrate significant benefits for T_C, it performed effectively in enhancing T_D when combined with CB and CF. A decline in both T_C and T_D was observed in samples containing 0.5 % CNT. Interestingly, the density of these samples did not exhibit the same trend; instead, it increased. This is contrary to the expectation that higher density would facilitate heat transport. This contradictory finding can be attributed to the quality of nano-material incorporation, particularly at elevated concentrations. In summary, both CNT and CB have the potential to enhance T_D, despite their differing effects on T_C. Therefore, it is not appropriate to characterise the addition of CNT as detrimental solely based on its unfavourable impact on T_C.

4.3. Mechanical performance

The final data is shown in Fig. 13. The reduction in strength observed in SC0 is a common issue associated with PCM concrete, as

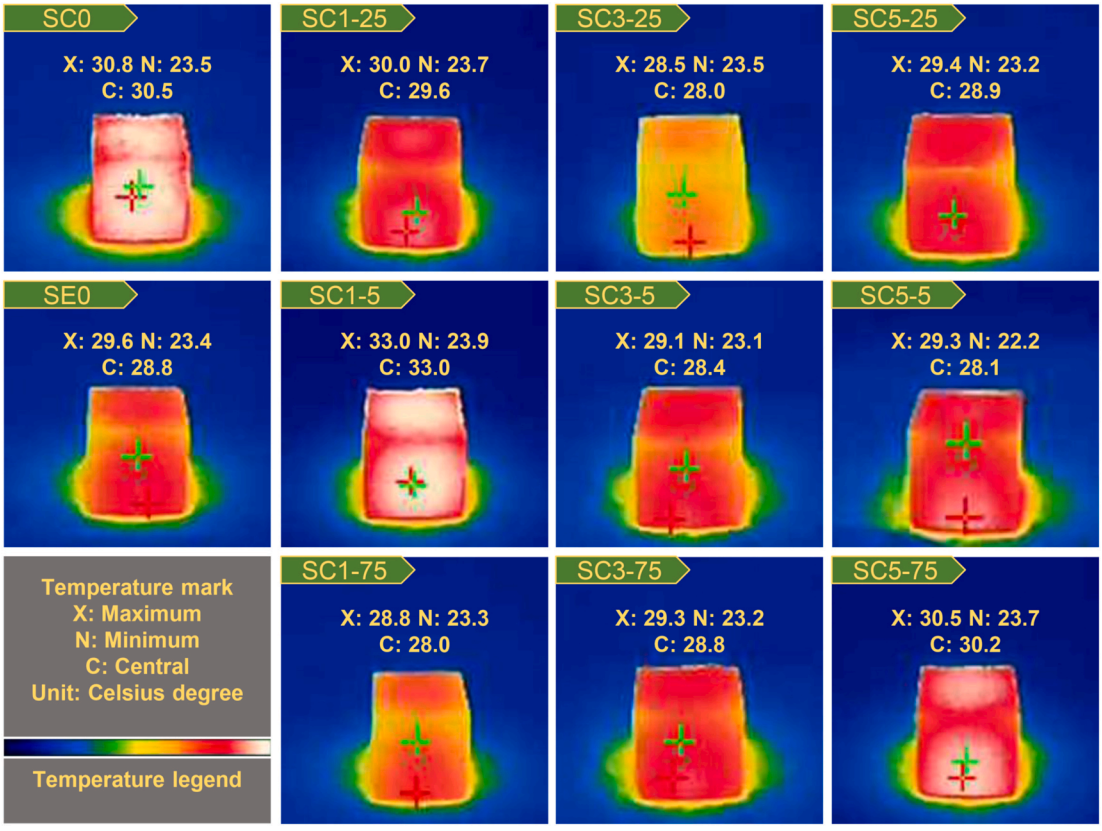

Fig. 6. Temperature distribution at 30 min cooling.

discussed in the previous section. The results indicate a notable decrease of 28 % compared to SE0. The benefits of incorporating carbon additives into the concrete matrix were generally significant. The trends in compressive strength closely mirrored the changes in density shown in Fig. 10, with clear enhancements evident across various samples. Only minor reductions in strength were noted in samples with minimal carbon additions, such as SC1-25 and SC1-5. The millimeter-scale CF may have disrupted the formation of a uniform bond between the cement paste and aggregates, adversely affecting both density and compressive strength. While CF was expected to improve concrete strength, the mixing strategy employed in this experiment resulted in insufficient bonding between the cement paste and CF at lower levels of nano-material addition. As the amount of carbon additions increased, the enhancements in strength became more pronounced, particularly starting from SC1-75, which demonstrated a moderate increase of approximately 10 %. This enhancement can be attributed to the synergistic effects of both nano- and millimeter-scale carbon materials. The effectiveness of CNT significantly increased within the range of 0.1 %–0.3 %. Although the continuous benefits of CB were observed at the same CNT content, the efficiency of CB was lower than that of CNT. With a constant quantity of CB, higher CNT concentrations resulted in increased strength, with optimal efficiency achieved at a CB level of 0.25 %. The highest compressive strength was recorded in SC5-75, followed closely by SC3-75, with the optimal formulation achieving a 24 % enhancement compared to SC0.

4.4. Thermal, compound, and structure characteristics

4.4.1. DSC

Several critical samples were selected to present the thermal properties based on DSC results as shown in Fig. 14. Both NS and NHP exhibited ideal enthalpy values of 295.6 J/g and 228.7 J/g, respectively, which were close to theoretical expectations. The conventional sample, like SE0, displayed no latent heat. While specific heat can store thermal energy, its efficiency is significantly lower than that of latent heat; however, the stable temperature associated with latent heat is particularly advantageous. Following the addition of PCM, SC0 exhibited clear latent heat. A notable difference compared to raw PCM was the increase in the number of peaks, which resulted from the moderate interaction between the two PCMs, where differing molecular forces influenced the combination and separation of water molecules. The melting point decreased to 28.2 °C, while the final endpoint rose above 53.7 °C. The endpoint of the first peak closely correlated with the start point of the second peak, demonstrating the continuity of the phase-changing effect. The melting range was significantly broader than that of raw PCMs, providing more favorable application conditions. The enthalpy of SC0 was remarkably lower than that of raw PCMs, around only one-tenth. Most of the enthalpy was contributed by the PCM, with conventional concrete components having minimal influence. Furthermore, as indicated in the mixing plan in Table 1, the mass of PCM

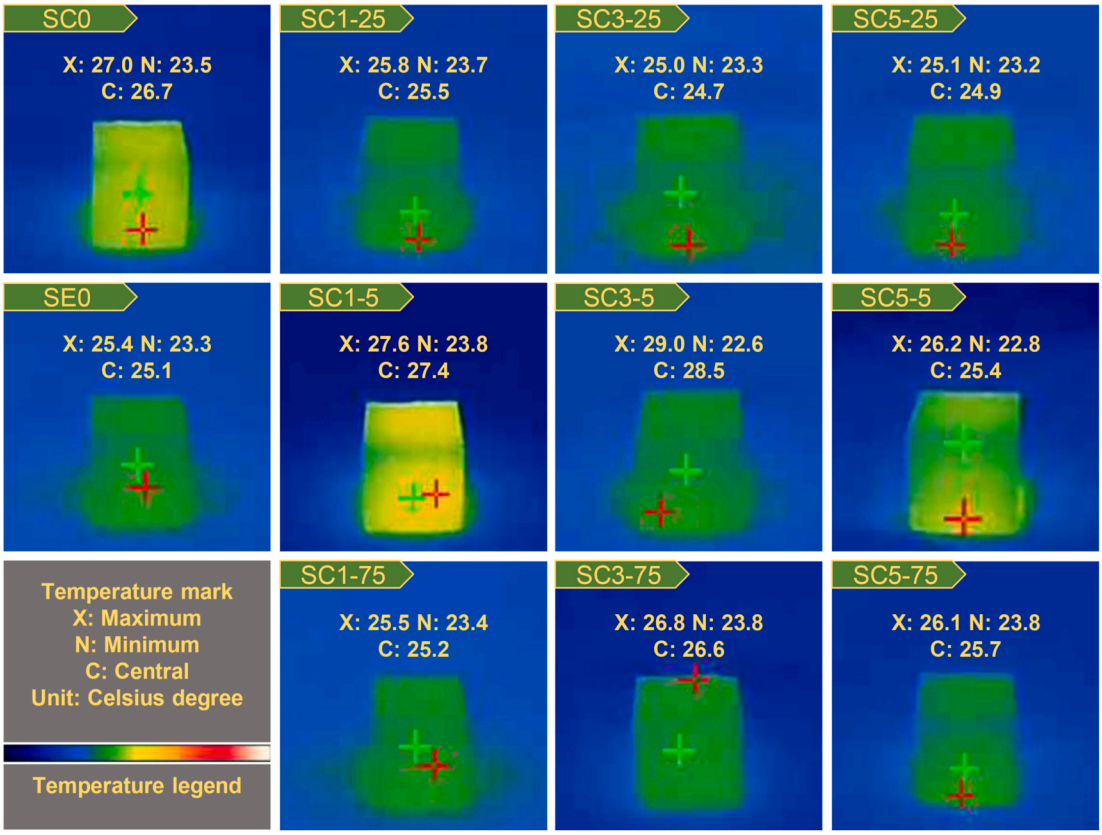

Fig. 7. Temperature distribution at 60 min cooling.

constituted only a small fraction of the total sample, thereby reducing overall enthalpy. Nevertheless, SC0 still exhibited substantial capacity for thermal energy storage.

4.4.2. XRD

The crystal characteristics of XRD are shown in Fig. 15 where the major peaks and corresponding products are labeled. Most samples with carbon additions showed similar peaks with the reference, and the variety of products remained consistent. The peak at around 42° corresponding to calcium silicate hydrate (C-S-H) was slightly diminished in the samples with carbon materials. A similar observation was made for the peak around 50° for C-S-H, although the SC5-25 group displayed a stronger peak in this region. Conversely, the primary peaks for C-S-H at approximately 29°, 33°, 36° and 45.5° were quite stable across samples. The peaks for portlandite were also stable even though fluctuation was observed at around 55° and 60°. Additionally, the peaks for quartz, ettringite, and calcite were remarkably stable, indicating minimal influence from the carbon materials. While differences in peak intensity were observed among the samples, both the positions and the number of peaks remained unchanged. It can be concluded that the incorporation of carbon materials did not produce significant effects on the mortar composition.

4.4.3. TGA

The mass loss of samples at elevated temperatures is shown in Fig. 16. While the number and position of the peaks were similar across samples, notable differences in their characteristics were evident. The total weights of carbon-based materials ranged from 0 % to 0.65 % based on the raw material proportions, which had a minimal effect on the TGA results. The influence of varying SP was doubled, which was in the range of 0.2 %–1.7 %, while it mostly was decomposed at the first loss peak. In contrast, the PCM accounted for approximately 3.75 wt% of the total weight, excluding SE0. The inorganic hydrated salt PCM experienced dehydration and moisture loss at the first peak. The peaks observed around 450 °C and 700 °C were attributed to the products of cement hydration.

For the first peak, SE0 demonstrated the highest stability, with a residual mass of 98 %, whereas other samples showed significantly lower values, below 96 %. In addition to the reasons presented in the last paragraph, it may be attributed to the increased production of ettringite, although the contribution may not be dominant. The primary reason for mass loss remained the dehydration reaction of the PCMs. As shown in Fig. 16(a), the mass loss for Portlandite across all samples was comparable between 420 °C and 470 °C. SE0 exhibited a mass loss of 1.5 %, which was greater than the approximately 1 % loss observed in other samples. Additionally, the mass loss between 600 °C and 700 °C varied from 2.7 % to 3.9 %, with SE0 presenting the lowest loss ratio. This suggests that SE0 contained less calcite, with a mass loss of 2.7 %, while other samples experienced calcite loss of about 3.5 %.

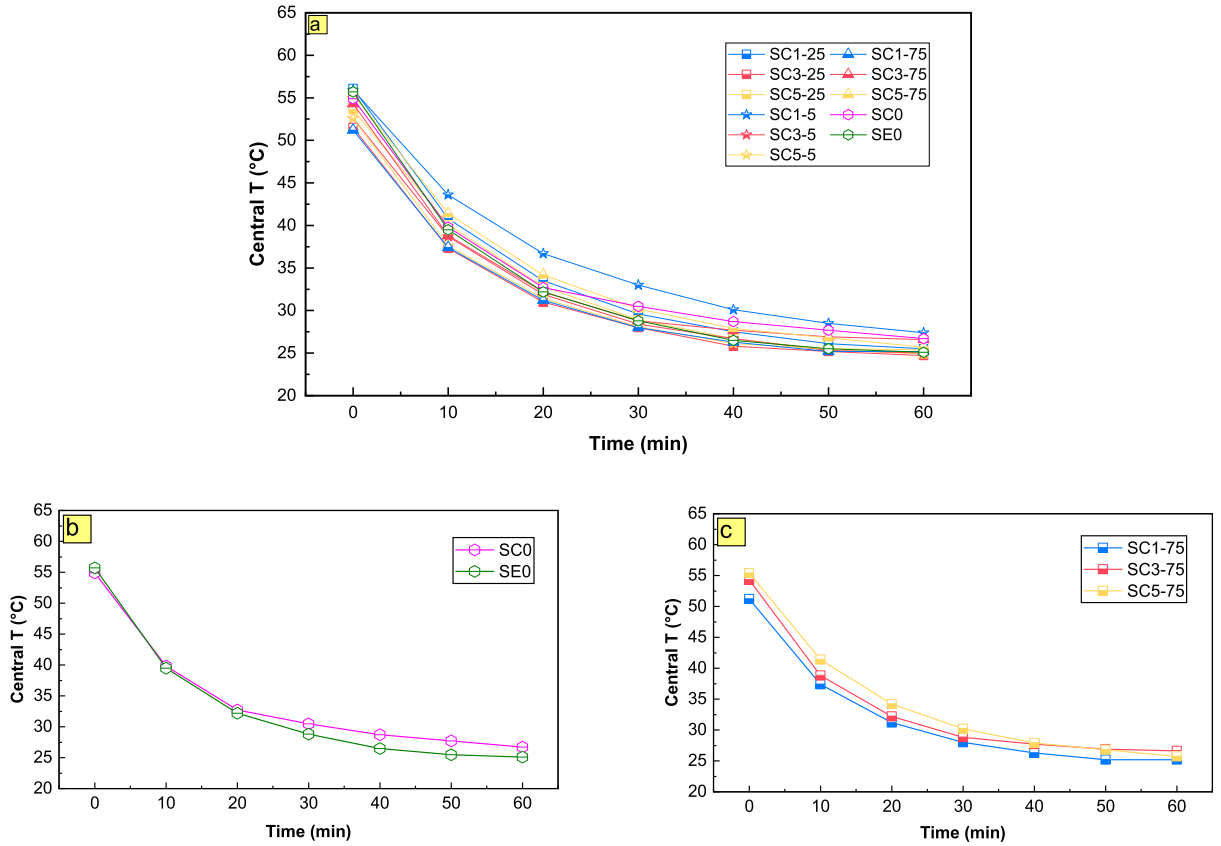

Fig. 8. Central point temperature development (a. Whole data; b. temperature development for SE0 and SC0; c. Typical temperature development with CB75).

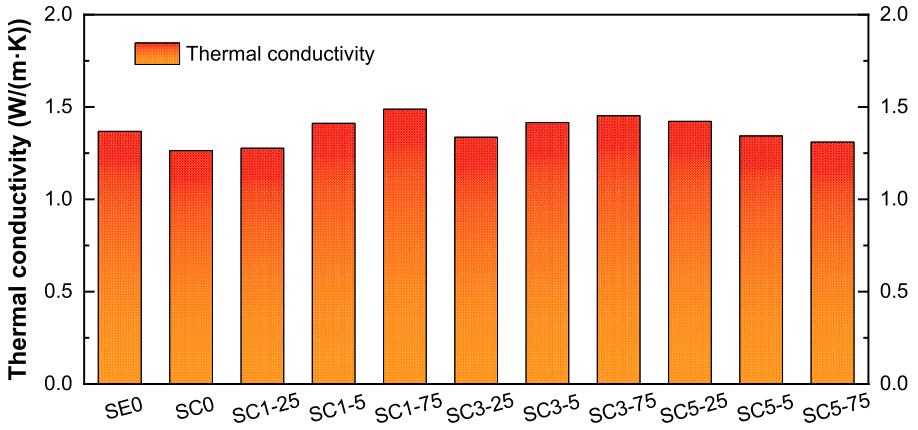

Fig. 9. Thermal conductivity in room temperature.

The derivative thermogravimetry (DTG) peaks displayed moderate similarity at high temperatures, with slight differences in starting and ending temperatures. This variation did not significantly affect the proportion of hydration products or the thermal stability of the samples. Ultimately, the mass of most samples stabilised at approximately 85 %, while SE0 reached around 88 %. The 3 % difference was consistent with the conditions observed after the first peak, indicating similar thermal stability at elevated temperatures.

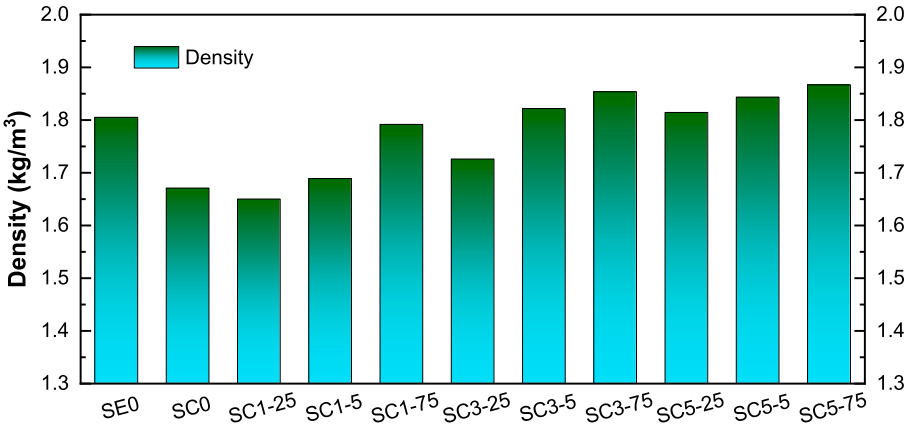

Fig. 10. Density of different specimens.

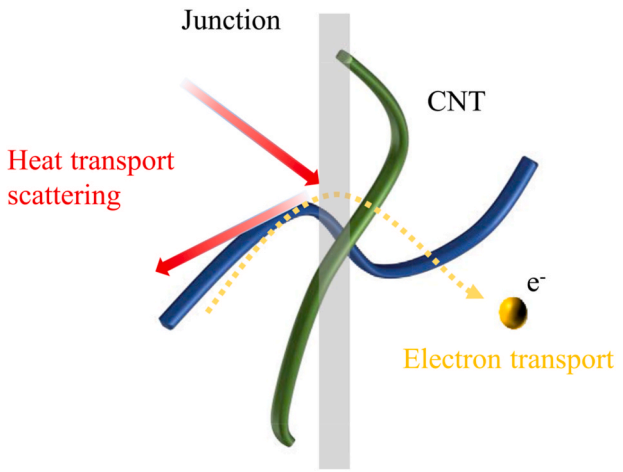

Fig. 11. Schematic diagram for thermal conduction [52].

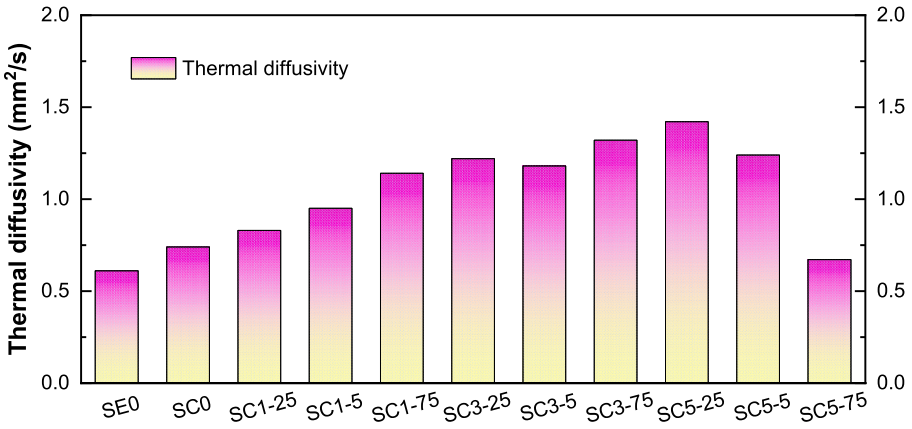

Fig. 12. Thermal diffusivity at room temperature.

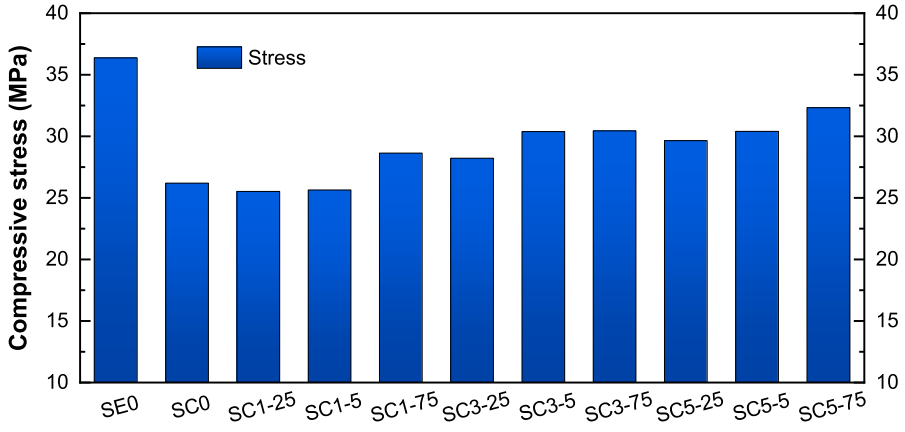

Fig. 13. Compressive strength at 28-day.

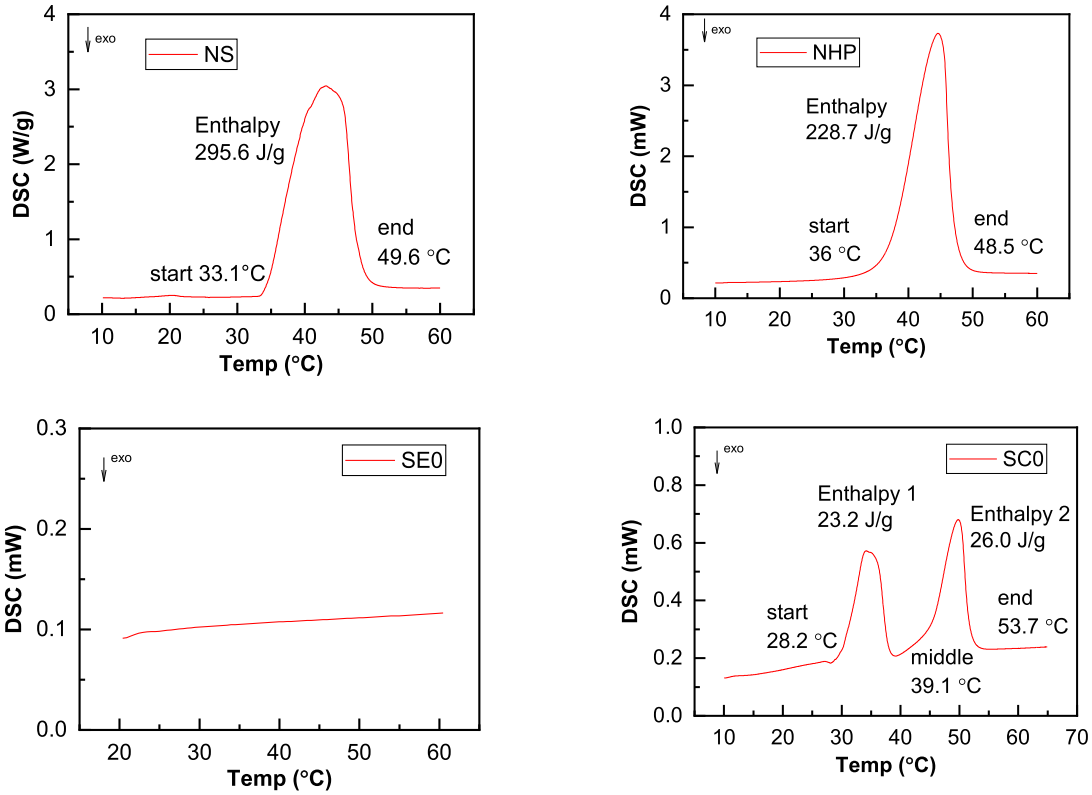

Fig. 14. DSC results and thermal properties of important materials.

4.4.4. Microstructure

Numerous properties discussed in the preceding sections are influenced by the microstructure; therefore, specific results from SEM are analysed in this section. As shown in Fig. 17, CFs were incorporated into the mortar. The CFs are significantly longer than other components, such as aggregates, and have the capacity to bridge cracks effectively. The images were captured from crushed samples that had undergone fracturing. Observations of scratches on the mortar surface and the broken faces of the CFs confirm the support provided by the fibers under applied stress. This microstructural effect is a key factor contributing to the enhanced mechanical properties observed in comparison to SC0. The subsequent analysis will focus on the further influence of various carbon materials.

As shown in Fig. 18 (a), cement hydration products and carbon materials can adhere to the CF surface, showing a stable connection. The CFs are capable of bridging discrete sections and extending through the sample at a millimeter scale, as mentioned in the previous

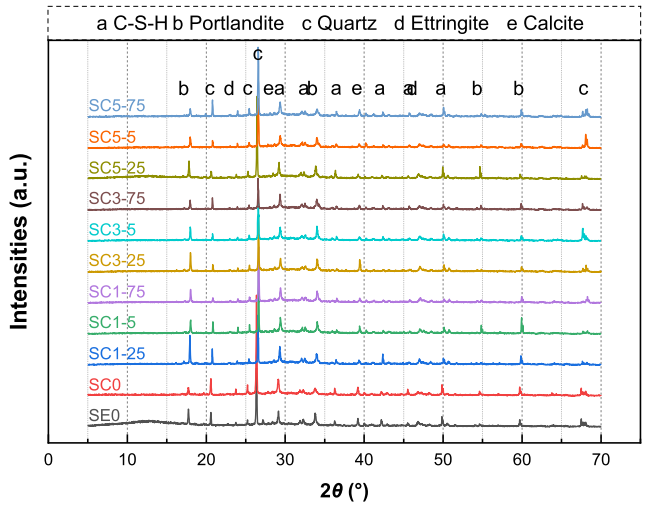

Fig. 15. XRD results of samples at 28d

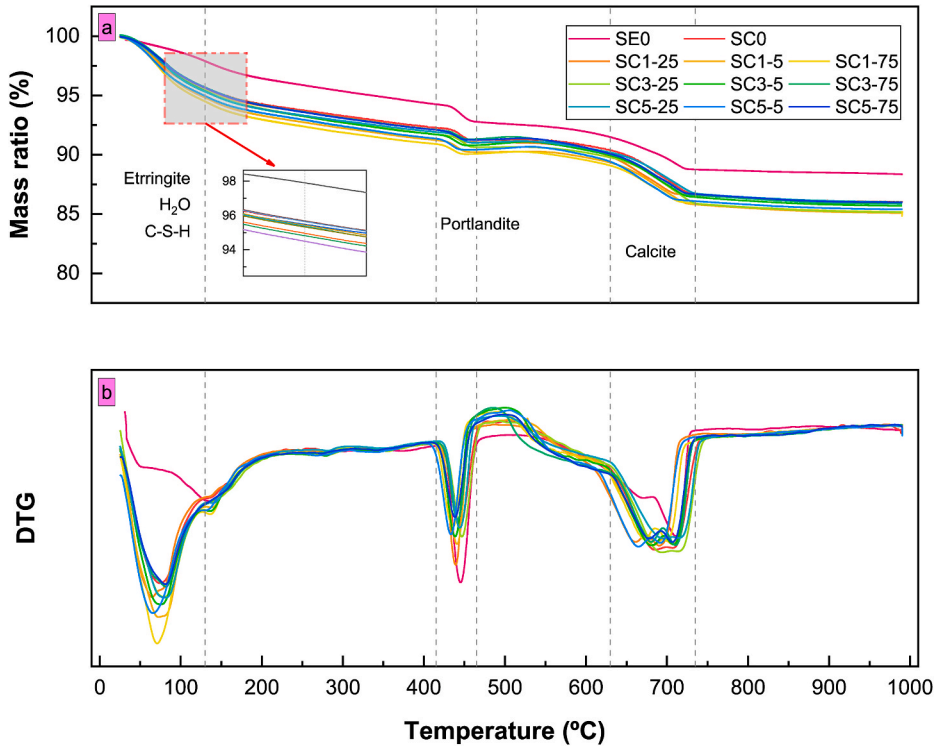

Fig. 16. TGA results of all groups (a. Thermal gravimetric; b. Derivative thermal gravimetric).

paragraph. Additionally, a long conductive path may be established by the CFs interacting with the attached materials, complementing the mechanical bonding. While both epoxy (EP) and CF are millimeter-sized, EP is fragile and non-conductive. The CF plays a significant role in enhancing both the mechanical and thermal properties at this scale. CNT and CB were incorporated into the cement hydration products and adhered to the CFs, thereby improving the mechanical and thermal properties of the cement paste [33]. However, excessive additions may disrupt the stability of the mortar. As shown in Fig. 18 (b), large agglomerates of CNT and CB can form clusters in specific areas. The enhancement of both mechanical and thermal properties was contingent upon the favourable distribution of the additions. Moreover, excessive carbon materials can compromise the stability of the cement hydration products. The SEM results corroborate the phenomena and analyses presented in 4.1, 4.2 and 4.3.

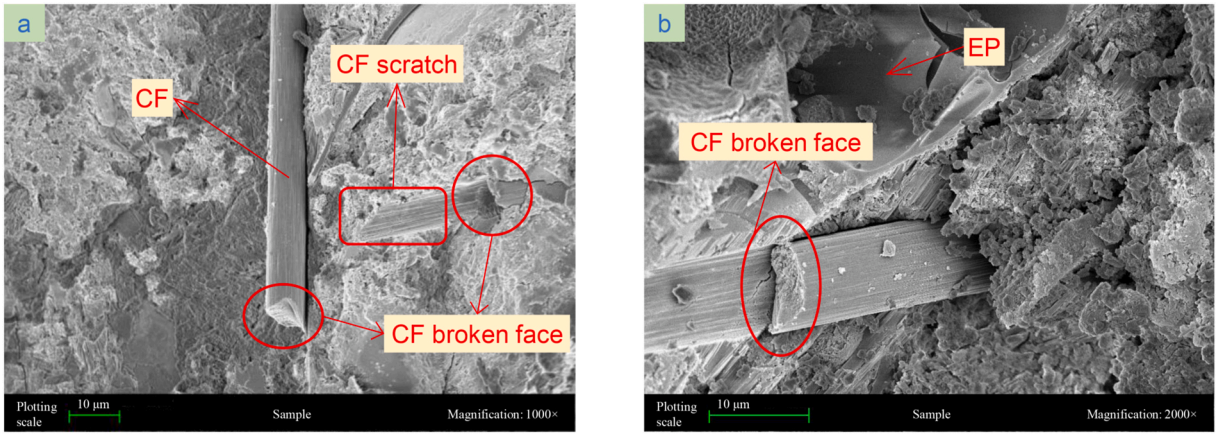

Fig. 17. Microstructure of specimens: (a) SC3-5 and (b) SC5-25.

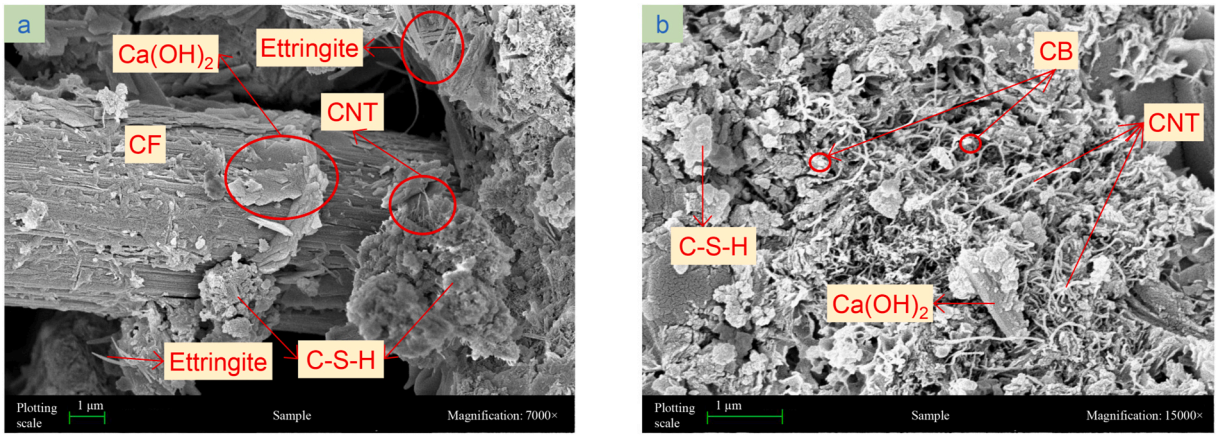

Fig. 18. Microstructure of specimens: (a) SC3-75 and (b) SC5-5.

5. Conclusions

This study developed a PCM mortar incorporating carbon materials and investigated its overall performance. The benefits of carbon additives in enhancing thermal transfer efficiency are substantial, although the mechanisms differ between the materials. CNT and CB modify the cementitious paste due to their nanoscale properties, impacting both thermal conductivity and mechanical performance. The structure of CNT may create cross-links that inhibit phonon movement. Additionally, the elongated form of CF provides a strong bridging effect. Beyond its conventional benefits for mechanical properties, CF facilitates the adhesion of CNT and CB, thereby establishing an extended thermal conduction path. The synergistic effects of these additives can yield significant advantages for PCM mortar. However, the optimal mass of each additive warrants careful investigation, as excessive amounts can have detrimental effects. The modification introduced by these carbon additives has minimal impact on thermal stability and the composition of the products. The main findings are summarized as follows:

(1) Temperature Distribution: The surface temperatures of the heated cubes are uneven, exhibiting higher temperatures predominantly in the central area. During the cooling period, the inner core of the cube supplies heat to the surface, resulting in a spherical temperature gradient. The total heat energy storage capacity of the PCM mortar is higher, leading to a slower rate of temperature decrease. After 1 h, the temperatures of all samples decrease to nearly room temperature, with SC0 showing a higher temperature of 1.6 °C at 60 min. A temperature lag of 10–20 min is observed.
(2) Effects of Additions: Most samples exhibit a faster temperature reduction with increased carbon additions, except when the addition levels are excessively high. In samples with 0.5 % CB, a higher amount of CNT results in a lower temperature reduction. While CNT demonstrates excellent thermal conductivity, its benefits are somewhat diminished due to energy barriers that inhibit phonon movement. However, CNT significantly enhances thermal diffusivity, affirming its value in PCM concrete.
(3) Thermal Conductivity: The benefits of CB on thermal conductivity are evident in most samples, with higher thermal conductivity achieved with increased CB content. An exception is observed in groups with a substantial amount of CNT. Similar to CNT,

increasing CB also notably enhances thermal diffusivity. Besides the activation effect of carbon materials, the absorption properties of the structure play an important role.

(4) Compressive Strength: The compressive strength of the mortar improves by 24 %. SEM results indicate that CF spans a large area of the mortar, connecting cracks and gaps. CNT and CB are enveloped in the paste, adhering to the CF and integrating with hydration products. This cooperation enhances both thermal convection and mechanical properties. However, achieving a well-distributed incorporation of nano-materials is challenging. Agglomeration occurs at high addition levels, hindering improvements and potentially resulting in adverse effects.

(5) Thermal Stability: The introduction of carbon materials and PCM results in unstable components that affect thermal stability at approximately 100 °C. The intrinsic properties of the raw materials are the primary contributing factors. Furthermore, a reduction in the proportion of portlandite and an increase in calcite confirm improved thermal stability at elevated temperatures.

6. Limitations and further perspectives

This paper makes significant contributions to the application of phase change materials (PCM) in construction materials; however, several limitations remain. The experiments were conducted in a laboratory setting, and the sample size does not accurately represent real-world applications, such as walls, ceilings, and floors. Consequently, the scale effect is uncertain. Additionally, the stable laboratory conditions in this research do not accurately reflect ambient climate conditions. Regarding the experimental methodology, temperature development data were collected solely from the sample surface. However, thermal transfer is a gradual process, and the temperature distribution within the inner structure is crucial for understanding the comprehensive effects.

To advance this research, future studies should be conducted under real climate conditions. Utilising a climate chamber with temperature programming is also a viable option, as it would enhance testing efficiency. The sample size can be increased as long as it remains compatible with the testing facilities. Moreover, employing advanced methods to capture the inner three-dimensional temperature distribution is essential, as this would help reveal precise thermal convection patterns and facilitate the development of numerical models.

CRediT authorship contribution statement

Xiaonan Wang: Writing – review & editing, Writing – original draft, Methodology, Investigation, Formal analysis, Data curation. **Yuhan Huang:** Writing – review & editing, Writing – original draft, Validation, Supervision. **Long Shi:** Writing – review & editing, Writing – original draft, Validation. **Shishun Zhang:** Validation, Writing – review & editing. **Wengui Li:** Writing – review & editing, Writing – original draft, Validation, Resources, Conceptualization.

Declaration of competing interest

The authors declare that they have no known competing financial interests or personal relationships that could have appeared to influence the work reported in this paper.

Acknowledgement

The authors acknowledge the support from Australian Research Council (ARC), Australia (FT220100177, LP230100288, DP220101051, DP220100036; IH200100010). The first author Xiaonan Wang also thanks the China Scholarship Council (CSC).

Data availability

Data will be made available on request.

References

[1] F. Farooq, X. Jin, M. Faisal Javed, A. Akbar, M. Izhar Shah, F. Aslam, R. Alyousef, Geopolymer concrete as sustainable material: a state of the art review, Construct. Build. Mater. 306 (2021) 124762.
[2] K. Kaspar, M. Ouf, U. Eicker, A critical review of control schemes for demand-side energy management of building clusters, Energy Build. 257 (2022) 111731.
[3] X. Wang, W. Li, Y. Guo, A. Kashani, K. Wang, L. Ferrara, I. Agudelo, Concrete 3D printing technology for sustainable construction: a review on raw material, concrete type and performance, Dev. Built Environ. 17 (2024) 100378.
[4] M. Arıcı, F. Bilgin, M. Krajčík, S. Nižetić, H. Karabay, Energy saving and CO2 reduction potential of external building walls containing two layers of phase change material, Energy 252 (2022) 124010.
[5] M. Saffari, C. Roe, D.P. Finn, Improving the building energy flexibility using PCM-enhanced envelopes, Appl. Therm. Eng. (2022) 119092.
[6] D. Abd El-Raheim, A. Mohamed, M. Fatouh, H. Abou-Ziyan, Comfort and economic aspects of phase change materials integrated with heavy-structure buildings in hot climates, Appl. Therm. Eng. 213 (2022) 118785.
[7] C. Arumugam, S. Shaik, Air-conditioning cost saving and CO2 emission reduction prospective of buildings designed with PCM integrated blocks and roofs, Sustain. Energy Technol. Assessments 48 (2021) 101657.
[8] A.I. Khdair, G. Abu Rumman, M. Basha, Developing building enhanced with PCM to reduce energy consumption, J. Build. Eng. 48 (2022) 103923.
[9] B. Lamrani, K. Johannes, F. Kuznik, Phase change materials integrated into building walls: an updated review, Renew. Sustain. Energy Rev. 140 (2021) 110751.

[10] H. Yang, Z. Xu, H. Cui, X. Bao, W. Tang, G. Sang, X. Chen, Cementitious composites integrated phase change materials for passive buildings: an overview, Construct. Build. Mater. 361 (2022) 129635.
[11] Y. Zhang, X. Sun, M.A. Medina, A reduced-scale experimental method for the thermal evaluation of building envelopes outfitted with phase change materials, J. Build. Eng. 62 (2022) 105372.
[12] D. García-Pérez, J. Xamán, I. Zavala-Guillén, Y. Chávez-Chena, E. Simá, J. Arce, Annual evaluation of a modified wall with PCM to reduce energy consumption and CO2 emissions in Southeast Mexico, Energy Build. 292 (2023) 113129.
[13] C. Baylis, C.A. Cruickshank, Economics and lifecycle carbon assessment of coconut oil as an alternative to paraffin phase change materials in North America, Energy Build. 294 (2023) 113268.
[14] J. Hirschey, M. Goswami, D.O. Akamo, N. Kumar, Y. Li, T.J. LaClair, K.R. Gluesenkamp, S. Graham, Effect of expanded graphite on the thermal conductivity of sodium sulfate decahydrate (Na2SO4·10H2O) phase change composites, J. Energy Storage 52 (2022) 104949.
[15] X. Sun, L. Liu, Y. Mo, J. Li, C. Li, Enhanced thermal energy storage of a paraffin-based phase change material (PCM) using nano carbons, Appl. Therm. Eng. 181 (2020) 115992.
[16] P. Talebizadehsardari, J.M. Mahdi, H.I. Mohammed, M.A. Moghimi, A. Hossein Eisapour, M. Ghalambaz, Consecutive charging and discharging of a PCM-based plate heat exchanger with zigzag configuration, Appl. Therm. Eng. 193 (2021) 116970.
[17] A. Pizzolato, A. Sharma, K. Maute, A. Sciacovelli, V. Verda, Design of effective fins for fast PCM melting and solidification in shell-and-tube latent heat thermal energy storage through topology optimization, Appl. Energy 208 (2017) 210–227.
[18] J.Y. Ho, Y.S. See, K.C. Leong, T.N. Wong, An experimental investigation of a PCM-based heat sink enhanced with a topology-optimized tree-like structure, Energy Convers. Manag. 245 (2021) 114608.
[19] A. Nematpour Keshteli, M. Sheikholeslami, Nanoparticle enhanced PCM applications for intensification of thermal performance in building: a review, J. Mol. Liq. 274 (2019) 516–533.
[20] D.G. Atinafu, B.Y. Yun, S. Wi, Y. Kang, S. Kim, A comparative analysis of biochar, activated carbon, expanded graphite, and multi-walled carbon nanotubes with respect to PCM loading and energy-storage capacities, Environ. Res. 195 (2021) 110853.
[21] X. Li, Y. Zhao, X. Min, J. Xiao, X. Wu, R. Mi, Y.g. Liu, Z. Huang, M. Fang, Carbon nanotubes modified graphene hybrid Aerogel-based composite phase change materials for efficient thermal storage, Energy Build. 273 (2022) 112384.
[22] H. Huang, L. Teng, K.H. Khayat, X. Gao, F. Wang, Z. Liu, For the improvement of mechanical and microstructural properties of UHPC with fiber alignment using carbon nanotube and graphite nanoplatelet, Cement Concr. Compos. 129 (2022) 104462.
[23] G. Li, L. Wang, J. Yu, B. Yi, C. He, Z. Wang, C.K.Y. Leung, Mechanical properties and material characterization of cement mortar incorporating CNT-engineered polyvinyl alcohol latex, Construct. Build. Mater. 345 (2022) 128320.
[24] Z. Wang, T. Shao, H. Zhang, J. Huo, J. Liu, T. Zhang, X. Ji, H. Zhang, J. Wang, H. Guo, P. Yu, Principles, properties and applications of smart conductive cement-based composites: a state-of-the-art review, Construct. Build. Mater. 408 (2023) 133569.
[25] M.A. Fikri, A.K. Pandey, M. Samykano, K. Kadirgama, M. George, R. Saidur, J. Selvaraj, N.A. Rahim, K. Sharma, V.V. Tyagi, Thermal conductivity, reliability, and stability assessment of phase change material (PCM) doped with functionalized multi-wall carbon nanotubes (FMWCNTs), J. Energy Storage 50 (2022) 104676.
[26] M.Z. Haider, X. Jin, J.W. Hu, Development of nanomodified-cementitious composite using phase change material for energy saving applications, Appl. Energy 340 (2023) 121067.
[27] B. Xu, Z. Li, Paraffin/diatomite/multi-wall carbon nanotubes composite phase change material tailor-made for thermal energy storage cement-based composites, Energy 72 (2014) 371–380.
[28] R. Fan, M. Wan, N. Zheng, Z. Sun, Simultaneously enhanced light absorption and heat transfer capability of melamine foam stabilized phase change composites by carbon black and metal fins for photothermal conversion and storage, J. Energy Storage 54 (2022) 105278.
[29] A.K. Mishra, B.B. Lahiri, J. Philip, Carbon black nano particle loaded lauric acid-based form-stable phase change material with enhanced thermal conductivity and photo-thermal conversion for thermal energy storage, Energy 191 (2020) 116572.
[30] Z. Guo, G. Sang, S. Zou, X. Cui, Y. Zhang, T. Guo, Thermo-mechanical properties of a novel carbon fiber modified self-encapsulated PEG/sulphoaluminate cement-based thermal energy storage composite, J. Build. Eng. 71 (2023) 106473.
[31] P. Singh, R.K. Sharma, G. Hekimoğlu, A. Sarı, O. Gencel, V.V. Tyagi, Expanded waste glass/methyl palmitate/carbon nanofibers as effective shape stabilized and thermal enhanced composite phase change material for thermal energy storage, J. Energy Storage 64 (2023) 107205.
[32] D. Lu, D. Wang, J. Zhong, Highly conductive and sensitive piezoresistive cement mortar with graphene coated aggregates and carbon fiber, Cement Concr. Compos. 134 (2022) 104731.
[33] W. Li, W. Dong, Y. Guo, K. Wang, S.P. Shah, Advances in multifunctional cementitious composites with conductive carbon nanomaterials for smart infrastructure, Cement Concr. Compos. 128 (2022) 104454.
[34] Y. Zhou, Y. Cao, H. Chen, R. Wu, H. Cheng, F. Luo, Q. Qian, Q. Chen, Q. Lin, Three-dimensional continuous network graphite nanosheets-based carbon foam supported stearic acid as effective shape-stabilized phase change material, J. Energy Storage 59 (2023) 106575.
[35] P. Singh, R.K. Sharma, M. Khalid, R. Goyal, A. Sarı, V.V. Tyagi, Evaluation of carbon based-supporting materials for developing form-stable organic phase change materials for thermal energy storage: a review, Sol. Energy Mater. Sol. Cell. 246 (2022) 111896.
[36] Q. Liang, D. Pan, X. Zhang, Construction and application of biochar-based composite phase change materials, Chem. Eng. J. 453 (2023) 139441.
[37] E. Baccega, M. Bottarelli, S. Cesari, Addition of granular phase change materials (PCMs) and graphene to a cement-based mortar to improve its thermal performances, Appl. Therm. Eng. 229 (2023) 120582.
[38] D.G. Atinafu, B.Y. Yun, Y. Kang, S. Wi, S. Kim, Three-dimensional hybrid carbon nanocomposite-based intelligent composite phase change material with leakage resistance, low electrical resistivity, and high latent heat, J. Ind. Eng. Chem. 98 (2021) 435–443.
[39] S. Ramakrishnan, X. Wang, J. Sanjayan, Effects of various carbon additives on the thermal storage performance of form-stable PCM integrated cementitious composites, Appl. Therm. Eng. 148 (2019) 491–501.
[40] Z. Rao, T. Xu, C. Liu, Z. Zheng, L. Liang, K. Hong, Experimental study on thermal properties and thermal performance of eutectic hydrated salts/expanded perlite form-stable phase change materials for passive solar energy utilization, Sol. Energy Mater. Sol. Cell. 188 (2018) 6–17.
[41] W. Dong, Y. Guo, Z. Sun, Z. Tao, W. Li, Development of piezoresistive cement-based sensor using recycled waste glass cullets coated with carbon nanotubes, J. Clean. Prod. 314 (2021) 127968.
[42] W. Li, Y. Guo, X. Zhang, W. Dong, X. Li, T. Yu, K. Wang, Development of self-sensing ultra-high-performance concrete using hybrid carbon black and carbon nanofibers, Cement Concr. Compos. 148 (2024) 105466.
[43] J. Cao, Y. He, J. Feng, S. Lin, Z. Ling, Z. Zhang, X. Fang, Mini-channel cold plate with nano phase change material emulsion for Li-ion battery under high-rate discharge, Appl. Energy 279 (2020) 115808.
[44] A. de Gracia, J. Tarragona, A. Crespo, C. Fernández, Smart control of dynamic phase change material wall system, Appl. Energy 279 (2020) 115807.
[45] X. Wang, W. Li, Z. Luo, K. Wang, S.P. Shah, A critical review on phase change materials (PCM) for sustainable and energy efficient building: design, characteristic, performance and application, Energy Build. 260 (2022) 111923.
[46] X. Wang, W. Li, Y. Huang, S. Zhang, K. Wang, Study on shape-stabilised paraffin-ceramsite composites with stable strength as phase change material (PCM) for energy storage, Construct. Build. Mater. 388 (2023) 131678.
[47] A. Karaipekli, A. Biçer, A. Sarı, V.V. Tyagi, Thermal characteristics of expanded perlite/paraffin composite phase change material with enhanced thermal conductivity using carbon nanotubes, Energy Convers. Manag. 134 (2017) 373–381.
[48] ASTM, C109/C109M - 21 Standard Test Method for Compressive Strength of Hydraulic Cement Mortars (Using 2-in. Or [50 Mm] Cube Specimens), ASTM International, West Conshohocken, PA, 2021.
[49] M.h. Dehmous, E. Franquet, N. Lamrous, Mechanical and thermal characterizations of various thermal energy storage concretes including low-cost bio-sourced PCM, Energy Build. 241 (2021) 110878.

[50] A. Yousefi, W. Tang, M. Khavarian, C. Fang, Development of novel form-stable phase change material (PCM) composite using recycled expanded glass for thermal energy storage in cementitious composite, Renew. Energy 175 (2021) 14–28.
[51] Y. Shen, S. Liu, C. Zeng, Y. Zhang, Y. Li, X. Han, L. Yang, X.e. Yang, Experimental thermal study of a new PCM-concrete thermal storage block (PCM-CTSB), Construct. Build. Mater. 293 (2021) 123540.
[52] K. Choi, D. Kim, W. Chung, C. Cho, S.-W. Kang, Nanostructured thermoelectric composites for efficient energy harvesting in infrastructure construction applications, Cement Concr. Compos. 128 (2022) 104452.
[53] W. Jin, C. Roux, C. Ouellet-Plamondon, J. Caron, Life cycle assessment of limestone calcined clay concrete: Potential for low-carbon 3D printing, Sustain. Mater. Technol. 41 (2024) e01119.
[54] R. Guo, C. Ou, L. Ma, Z. Long, F. Xu, C. Yin, Experimental study on impact performance of seawater sea-sand concrete with recycled aggregates, Sustain. Mater. Technol. 41 (2024) e01060.
[55] G.M. Zannerni, K.P. Fattah, A.K. Al-Tamimi, Ambient-cured geopolymer concrete with single alkali activator, Sustain. Mater. Technol. 23 (2020) e00131.
[56] Q. Wu, Y. Huang, P. Irga, P. Kumar, W. Li, W. Wei, H.K. Shon, C. Lei, J.L. Zhou, Synergistic control of urban heat island and urban pollution island effects using green infrastructure, J. Environ. Manag. 370 (2024) 122985.
[57] K. Yang, G. Long, Z. Tang, W. Li, G. Ma, C Li, Y. Xie, Enhancing the flexural toughness of UHPC through flexible layer-modified aggregates: A novel interfacial toughening strategy, Cem. Concr. Compos. 154 (2024) 105770.
[58] W. Dong, S. Gao, S. Peng, L. Shi, S.P. Shah, W. Li, Graphene reinforced cement-based triboelectric nanogenerator for efficient energy harvesting in civil infrastructure, Nano Energy 131 (2024) 110380.
[59] Q. Liu, A. Cheng, C. Sun, K. Chen, Y. Wang, W. Li, Effects of aggregate's type and orientation on stress concentration and crack propagation of modeled concrete applied a shear force, J. Build. Eng. 95 (2024) 110340.
[60] Y. Lu, Y. Xu, L. Meng, F. Ouyang, J. Cheng, P. Duan, Y. Zhu, W. Li, Z. Zhang, M. Chen, W. Huang, Role of modified calcium montmorillonite and 5 A zeolite in microstructure and efflorescence formation of metakaolin-based geopolymer, Constr. Build. Mater. 448 (2024) 138258.